



**HAL**  
open science

# X-ray photoemission spectroscopy applied to nanodiamonds: From surface chemistry to in situ reactivity

Jean-Charles Arnault

► **To cite this version:**

Jean-Charles Arnault. X-ray photoemission spectroscopy applied to nanodiamonds: From surface chemistry to in situ reactivity. *Diamond and Related Materials*, 2018, 84, pp.157 - 168. 10.1016/j.diamond.2018.03.015 . cea-01773658

**HAL Id: cea-01773658**

**<https://cea.hal.science/cea-01773658>**

Submitted on 17 Apr 2023

**HAL** is a multi-disciplinary open access archive for the deposit and dissemination of scientific research documents, whether they are published or not. The documents may come from teaching and research institutions in France or abroad, or from public or private research centers.

L'archive ouverte pluridisciplinaire **HAL**, est destinée au dépôt et à la diffusion de documents scientifiques de niveau recherche, publiés ou non, émanant des établissements d'enseignement et de recherche français ou étrangers, des laboratoires publics ou privés.

# X-ray Photoemission Spectroscopy applied to Nanodiamonds: from surface chemistry to *in situ* reactivity

J. C. Arnault

CEA, LIST, Diamond Sensors Laboratory, F-91191 Gif-sur-Yvette, France.  
Corresponding author: jean-charles.arnault@cea.fr

## Abstract

The surface chemistry governs most of the physical and chemical properties of nanodiamonds (NDs). X-ray photoemission spectroscopy is a method of choice to characterize the surface of NDs. The present paper reviews on XPS studies focusing on modifications of surface terminations or grafting of biomolecules and polymers on NDs. The second part illustrates studies in which XPS can even be used as a specific tool to investigate *in situ* the reactivity and the stability of NDs towards various atmospheres like plasma or UHV annealing.

**Keywords** Nanodiamonds; X-ray Photoemission Spectroscopy; Surface reactivity; Functionalization;

## Introduction

Nanodiamonds (NDs) have attracted raising interests from research groups and companies within the last ten years. NDs can be obtained by crushing from bulk diamond grown by High Pressure High Temperature (HPHT) or Chemical Vapor Deposition (CVD) or by detonation synthesis [1]. Indeed, NDs gathers very different physical and chemical properties combining some expected from bulk diamond with new ones conferred by the nanoscale. In particular, surface effects were found to be exalted due to the high surface to volume ratio (5 nm detonation NDs behave a specific surface area of 400 m<sup>2</sup>/g). Surface chemistry is often the key governing this surface reactivity [2]. Moreover, the rich carbon chemistry provides various pathways to graft molecules of interest on NDs. This is specially required for applications of NDs in biology [3, 4], polymer composites [5] or lubricants [6].

Depending on the nature of functional groups present at their surface, NDs can possess negative or positive zeta potential in aqueous suspensions. Different models have been proposed to relate these opposite values to the surface chemistry of oxidized, hydrogenated or graphitized NDs [7, 8]. In addition, a control of the surface terminations can improve the colloidal stability of NDs in various media. Moreover, recent findings have demonstrated that NDs can act as active particles under X-ray illumination. A radiosensitization effect has been *in vitro* demonstrated in human radioresistant cancer cells under gamma irradiation [9]. A specificity of plasma hydrogenated NDs suspended in water was evidenced in terms of hydroxyl radicals overproduction under X-rays compared to oxidized NDs [10].

For all the previous reasons, it is essential to perform an extended analysis of the surface chemistry of NDs to better understand their reactivity in different atmospheres and media. Among available techniques, X-ray Photoemission Spectroscopy (XPS) also known as Electron Spectroscopy for Chemical Analysis (ESCA) behaves a place of choice. Indeed, it was regularly used for bulk diamond to investigate the sp<sup>3</sup> / sp<sup>2</sup> carbon ratio, the doping with boron, nitrogen or phosphorous, the surface terminations or grafted molecules at diamond surface. XPS was particularly powerful to monitor the changes in surface electronic properties of diamond surfaces. For hydrogenated surfaces of single crystalline diamond, it evidenced a negative electron affinity (NEA) [11] whereas it was involved to demonstrate the formation of a surface conductive layer (SCL) after adsorption of molecules onto the H-diamond surface [12].

The present paper reviews what XPS techniques have brought to the characterization of nanodiamonds. After a brief presentation of its principle, it situates XPS capabilities versus other characterization techniques like FTIR, TDMS, HRTEM, Raman or NMR. The artefacts linked to the XPS analysis of nanoparticles with sizes smaller than 10 nm are discussed. XPS studies of NDs which have underwent modifications of their surface either to induce different terminations or to graft molecules of interest will be reviewed. In a last part, the ability of XPS to sequentially investigate the reactivity of NDs toward different atmospheres will be illustrated with experiments performed without air exposure of the samples. Finally, the future development of the XPS technique will be discussed with advanced set-ups carried out in ambient conditions or on synchrotron facilities.

## 1. The XPS technique

XPS is nowadays a well-established characterization technique based on the photoelectric effect evidenced by Hertz in 1887 [13]. More details about its development since the mid-1960's and its complementarity with Auger Electron Spectroscopy (AES) were previously reviewed [14-17]. XPS can be combined with Synchrotron radiation for an improvement of the energy resolution due to the high flux of photons and a tunable photon energy [18]. Further developments of XPS like photoelectron diffraction and holography were recently reported to study complex interfaces [19] or to investigate the reactivity at solid/liquid interface for electrochemistry [20]. Nowadays, X-ray photoemission can even be performed under high ambient pressure [19].

### 1.1 What can be measured by XPS?

The XPS technique provides an indirect calculation of the binding energy (BE) of photoelectrons via the measurement of their kinetic energy (KE) using an electrostatic analyzer (Figure 1).

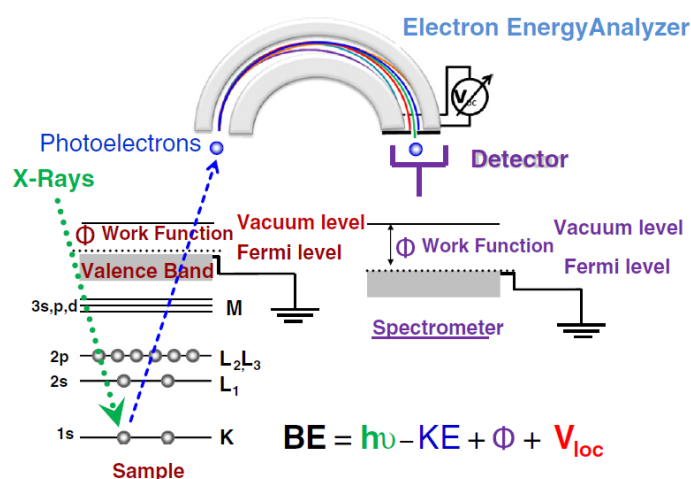


**Figure 1** XPS principle from [21].  $h\nu$  is the energy of incident photons, BE and KE are the binding and kinetic energies of photoelectrons,  $\phi$  the analyzer work function,  $V_{loc}$  the local electrical potential.

First, XPS permits to assess the chemical composition of the sample. All chemical elements except hydrogen and helium can be probed. The atomic concentration for each element is calculated using the corresponding photoelectric cross-section with depends on the original electronic state of the photoelectron and the incident photon energy [22]. For an element, the BE of a given electronic state will also vary versus the binding state of this element. The measurement of these chemical shifts is very helpful to identify binding states of elements.

Types of bonds	Binding energy (eV)	references
Si-C	282.7	[23]
C-C in diamond	284.5	[24]
C-C in B-doped diamond	283.8	
ligand (Ru complex)	285.3	
COOH	287.8	
C-F	289.3	

**Table 1:** Binding energies at C1s for different materials or surface terminations of diamond films, The same XPS set-up (monochromatic Al K $\alpha$  source) was used in the same conditions.

As an illustration, Table 1 provides values of BE for the carbon 1s core level either for different binding states of carbon in bulk materials (SiC, diamond) or to different terminations of diamond surfaces. Chemical shifts correspond to BE difference from few tenth of eV up to 10 eV [14].

The probed depth depends on the photon KE, the set-up geometry and the sample nature. Indeed, the material and the KE of photoelectrons significantly influence the inelastic mean free path (IMFP) for photoelectrons in the sample [25]. Typically, this depth is included between 1 nm to 20 nm. For this reason, XPS is most often cited as a surface analysis technique. Playing with the collection angle of photoelectrons toward the analyzer, the analyzed depth can be tuned. This is the basis for Angle Resolved XPS technique (ARXPS) [19].

Physical and chemical effects which could enter in the interpretation and analysis of XPS spectra were previously reviewed [26]. Some mechanisms like charge accumulation may lead to binding energy shifts. To limit charging effects, the use of a beam of low-energy electrons and/or ions ensures a charge compensation [27]. In that case,  $V_{loc}$  can be neglected in the calculation of the binding energy (Figure 1). On the other hand, electrical or optical signals can be applied to the sample during XPS measurements [21]. Induced BE shifts are used to investigate dopant nature, interfacial charges or photoinduced charge accumulation.

Details concerning the fitting of XPS data could be found elsewhere [14]. The quantification of XPS and AES data must also consider the energy losses of photoelectrons in the solid matrix, especially, the elastic scattering of electrons. These losses have been calculated via Monte Carlo simulations [28, 29]. During their path into the matter, photoelectrons also underwent energy losses by inelastic scattering. Among the likely mechanisms, the interaction of photoelectrons with the electrons cloud lead to quantified energy losses called plasmon loss peaks (XEELS). These structures recorded on the XPS spectra could be exploited in combination with core levels spectra to investigate diamond surfaces [23, 30]. XEELS spectra have been used to investigate *in situ* the reactivity of NDs under plasma or annealing (Part 3.2).

X-rays excited AES transitions (XAES) could be also collected on XPS spectra. The C KVV transitions are very sensitive to the electronic configuration of carbon as two electrons from the valence band are involved [31]. The use of X-rays excitation instead of electrons for AES prevents damages of the sample during experiments. As a consequence, the fingerprint of carbon surface structure is better obtained using XAES [32]. XAES and XPS studies were previously combined to compare the electronic structure of different carbon materials (graphene, graphite, diamond) [33].

The Ultra-Violet Photoemission Spectroscopy (UPS) is based on the XPS principle, conventional anodes (Al or Mg K $\alpha$ ) are then replaced by He I and He II rays at 21.2 and 40.8 eV, respectively. Using UPS, it is possible to probe the valence band of the analyzed sample. Such study has been reported for diamond surfaces [34], especially to measure the electron affinity for different terminations of diamond surfaces, especially hydrogenated and oxidized [35].

## 1.2 XPS compared to other characterizations techniques

In this paragraph, the assets of XPS technique are compared with those of other characterization techniques (Table 2).

	XPS	FTIR	HREELS	NMR	SIMS	ICP-MS
<b>Elemental analysis</b>	yes*	no	no	yes	yes	yes
<b>Detection limit</b>	0.1 at %	ppm	0.01% of a ML**	0.1 wt %	ppm-ppb	$10^{-7}$ - $10^{-11}$ wt. %
<b>Quantitative analysis</b>	yes	no	no	no	yes	yes
<b>Binding state</b>	yes	yes	yes	yes	no	no
<b>Destructive method</b>	no	yes	no	no	yes	yes
<b>Probed depth</b>	1-20 nm	whole sample	1-2 layers	whole sample	few $\mu\text{m}$	whole sample

\* except H and He; \*\*ML: monolayer

**Table 2:** Comparison of different techniques for material analysis

### ***Probed depth***

As already underlined, XPS belongs to surface analyses. The first nanometers of the sample are probed and ARXPS allows to tune this depth to achieve a profile analysis. Nevertheless, other techniques like High Resolution Electron Energy Loss Spectroscopy (HREELS) [36], Attenuated Total Reflectance (FTIR ATR) [37] or AES [17] are probing the extreme surface (upper 2-3 atomic planes).

### ***Detected elements and limit of detection***

XPS is not sensitive to light elements like hydrogen or helium. Secondary-ion mass spectroscopy (SIMS) [38] or neutron scattering are techniques which could allow to probe hydrogen in materials [39]. The detection limit of XPS is dependent on probed elements. Indeed, photoionization cross-sections could be very different from an element to another. For example, using an Al K $\alpha$  anode, these cross-sections are 0.8 for Si 2p and 25.4 for Cu 2p (in units of the C1s cross section which is 13600 barns [22]). The order of magnitude for XPS detection limit is around 0.1 at. %. In diamond films, XPS allows to measure boron concentrations for highly doped films ([B] $\sim 10^{21}$  atoms/cm<sup>3</sup>). As a consequence, lower boron concentrations cannot be detected contrary to SIMS or Cathodoluminescence techniques. To detect impurities in the range  $10^{-7}$  –  $10^{-11}$  wt. %, Inductively Coupled Plasma Mass Spectrometry (ICP-MS) is a method of choice (Table 2). It has been extensively used to quantify metallic impurities in nanodiamonds [40].

### ***Surface chemistry***

With XPS, it is possible to assess the surface terminations of the sample, according to the chemical shifts observed for different binding states (Table 1). On diamond surfaces, this has been exploited to discriminate different oxygen functional groups like ethers, carbonyls, carboxyls by analysis of carbon and oxygen core levels [41]. However, it remains difficult to obtain a quantitative analysis for these different chemical groups because of assumptions needed in spectrum fitting. Thermogravimetric Analysis (TGA), ATR and FTIR techniques appear very complementary to XPS for such analysis (Table 2). Thermal Desorption Mass Spectrometry (TDMS) is also powerful to identify functional groups according to their different binding states leading to different desorption temperature under vacuum [42]. In the literature, XPS is often used in combination with other techniques. For example, solid-state magnetic nuclear resonance (NMR) was used to probe surface hydrogenated groups and sp<sup>2</sup> carbon in detonation NDs [43]. The surface oxidation

of diamond (100) surfaces was investigated by XPS in combination with SIMS, UPS and Rutherford backscattering spectroscopy (RBS) [44]. To fully characterize the surface chemistry of nanoparticles (NPs), Nuclear Magnetic Resonance (NMR) spectroscopy is often coupled with XPS and FTIR [45].

### **Profile**

XPS used in angle resolved XPS mode (ARXPS) can bring a non-destructive depth profiling [16]. It constitutes an important advantage compared to alternative techniques based on ions: RBS or SIMS (Table 2). Secondly, XPS is less sensitive to surface roughness which could induce shadowing effects. Moreover, ARXPS avoids preferential sputtering or interface mixing, phenomena occurring during SIMS measurements. As a consequence, simulations taking into account these mechanisms should be used to interpret SIMS data for the analysis of nanometric layers [46]. Results obtained by ARXPS were compared in details with other techniques for profiling [47].

### **$Sp^2/sp^3$**

The carbon hybridisation states in bulk materials can be studied from C1s core level. Nevertheless, a recent report by Fujimoto et al. underlines the strong effect of surface charging on the assignation of  $sp^2$  and  $sp^3$  contributions in XPS C1s spectra [48]. According to the experiments and calculations done on 1  $\mu\text{m}$  diamond particles embedded in highly oriented pyrolytic graphite (HOPG), the carbon  $sp^3$  component may be located at a lower BE compared to the  $sp^2$  one. Such observation is not been yet taken into account for XPS studies of nanodiamonds. XEELS characterization is also sensitive to  $sp^2$  carbon ( $\pi$  fingerprint). The shape of C KVV Auger transitions allows to quantify the  $sp^2/sp^3$  ratio through the calculation of D parameter [31]. XAES reveals extremely powerful to quantify the graphene structure and the hydrogenated bulk diamond [33]. Up to now, such XAES studies have been rarely applied to diamond nanoparticles (Part 3.1).

## **1.3 XPS to analyze nanoparticles**

XPS is a pertinent technique to characterize nanoparticles (NPs) which are synthesized for different fields of applications, for example in biology or catalysis. Indeed, it gives access to their chemical composition and to their surface chemistry, both are strongly influencing the properties of NPs. Nevertheless, the size of NPs may induce significant changes in XPS spectra and can affect the intensity and the binding energies of XPS peaks. The inelastic background seems to be also affected in case of nanostructured sample [49].

For NPs having a size lower than 10 nm, effects on XPS intensity have been evidenced [50]. Indeed, these sizes are comparable to the mean free path of photoelectrons in the material. This means that the whole particle is probed and this leads to an exaltation of the surface contribution to the XPS signal (Figure 2).

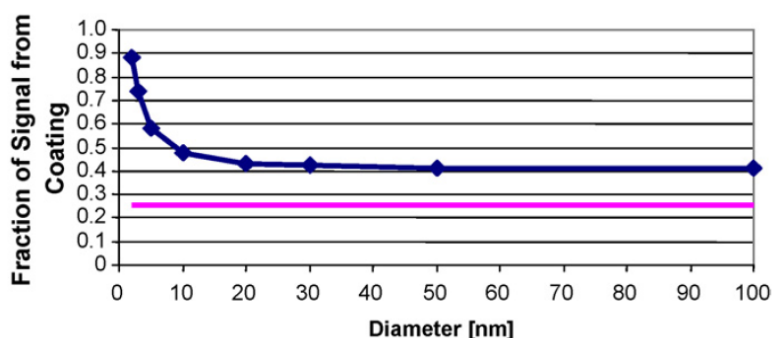


**Figure 2** Evolution of the XPS signal from the surface versus the diameter of spherical particles (from [50]). The curve in pink corresponds to a flat coating.

In that case, shape effects should be included in the XPS data exploitation. These aspects are particularly critical to estimate the thickness of an external shell in core-shell structures. Gold/Silver core-shell NPs were characterized by a combination of Scanning Transmission Electron Microscopy (STEM) and XPS including simulations of the spherical multilayer [51]. Models have been also developed to access the size of NPs [52, 53]. In addition, previous works have reported up-shifts for binding energies of elements in a nanostructured form compared to bulk one [54]. This effect was also observed in C1s spectra for diamond nanoparticles compared to diamond thin film grown by CVD (Figure 3). The C1s peak is broader (Full Width Half Maximum of 2.9 eV) for detonation NDs and up-shifted by 5 eV compared to the diamond film. A review comparing techniques allowing surface characterization of nanoparticles has been published by Baer et al [55].

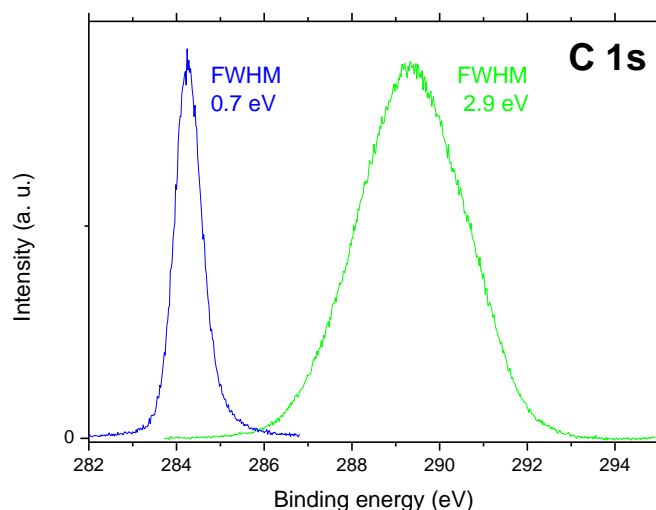


**Figure 3** Carbon core levels for a thin diamond film grown by CVD (in blue) and for 5 nm detonation NDs (in green), peaks have been normalized in intensity

## 2. XPS for characterization of NDs

The XPS technique was regularly used for the characterization of raw materials either produced by detonation or HPHT synthesis to measure the concentrations of impurities included in NDs (Part 2.1). Currently, NDs are deposited on a substrate starting from a colloidal suspension. To limit the charging effects, a control of the thickness of deposited NDs is needed. Spin coating is usually preferred to the drop casting. Many attempts were reported for the control of a homogeneous surface chemistry by means of chemical or physical treatments [2, 56]. XPS allows to monitor the modifications induced by these treatments at the surface of NDs (Part 2.2). Surface modified NDs usually serve as a basis for grafting of biomolecules or polymers. XPS is one of the techniques needed to characterize the grafted molecules (Part 2.3).



## 2.1 As received material

For raw NDs, XPS permits to measure the atomic concentrations of impurities. As previously underlined (Part 1), only elements with atomic content higher than 0.1 at. % are detectable. Oxygen and nitrogen are the common impurities reported in XPS analysis of as received NDs. The nitrogen concentration is included between 1 and 6 at. % depending on the source of NDs and the synthesis method: HPHT [57] or detonation [58, 59]. Oxygen concentration strongly depends on purification steps (mainly acid treatments) applied to raw NDs to remove amorphous or graphitic carbon and metallic impurities [59]. To quantify these impurities present at lower concentrations (range  $10^{-7}$  –  $10^{-11}$  wt. %), ICP-MS [40] or Laser-induced breakdown spectroscopy (LIBS) [60] are frequently used.

The combined analysis of C1s and N1s or O1s core levels brings useful informations about the binding state of nitrogen or oxygen at the NDs surface [61]. FTIR is an excellent complementary method to better investigate the nature of oxygen and nitrogen functional groups at the surface [62]. In some cases, other impurities like silicon or chlorine were reported in XPS analysis of NDs [57, 60-61]. For NDs produced by milling of boron doped diamond films grown by CVD, the concentration of dopants is usually insufficient to be detected with XPS ( $< 10^{21}$  atoms/cm<sup>3</sup> i. e. lower than 1 at %). For such NDs, the boron was indirectly detected by the Fano resonance observed in Raman spectroscopy which indicates a boron concentration higher than  $10^{20}$  atoms/cm<sup>3</sup> [62]. Moreover, EELS spectra recorded in HRTEM microscope confirmed the incorporation of boron in tetrahedral configuration in the diamond lattice [63].

Finally, the XPS analysis of raw NDs allows to investigate the carbon core level and to determine the fraction of sp<sup>3</sup>/sp<sup>2</sup> carbon. Nevertheless, as previously mentioned (Part 1.3), artefacts related to the small size of NDs, especially for detonation NDs, lead to shifts in position and broadening of the C1s peak. These effects complicate the fitting of C1s peaks compared to diamond films.

## 2.2 Surface modified nanodiamonds

During the last ten years, different surface treatments using physical (annealing, plasma) or chemical means were reported to ensure a more homogeneous surface chemistry for NDs [2]. XPS was often performed in combination with FTIR, TDMS, NMR or High Resolution TEM to characterize the induced surface modifications. Main results will be summarized in this paragraph.

### *Hydrogenation*

Two hydrogenation methods were developed to reduce oxygen functional groups at NDs surface: one based on microwave plasma, the other using an annealing under hydrogen atmosphere [64]. XPS was used to measure the reduction of oxygen functional groups after microwave plasma exposure [57] or after annealing under hydrogen [66]. The reduction of oxygen groups after plasma hydrogenation was confirmed by the comparison of the carbon core levels for HPHT NDs which confirmed the loss of C-O and C=O bonds present at higher binding energy (Figure 4a). A study of plasma hydrogenated detonation NDs by UPS revealed a slightly negative electron affinity (NEA) while oxidized NDs exhibited a positive electron affinity before hydrogenation [67]. This NEA, characteristic of hydrogenated diamond bulk surfaces, was more recently confirmed for detonation NDs after plasma hydrogenation using Scanning Tunneling Spectroscopy (STS) [68].

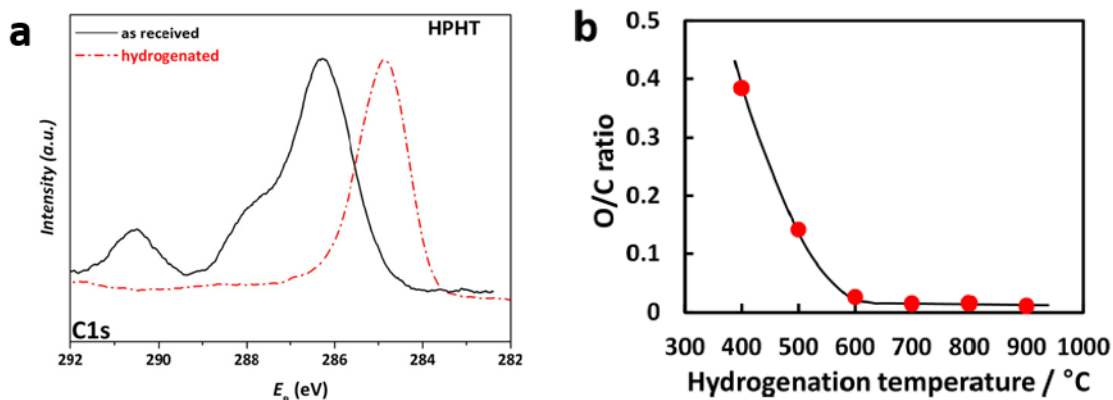


**Figure 4** a) Comparison of C1s core levels for HPHT NDs before and after plasma hydrogenation from [57] b) Evolution of O/C ratio versus the annealing temperature for hydrogenation of detonation NDs from [66]

For the annealing under hydrogen of detonation NDs, the oxygen to carbon ratio extracted from C1s and O1s showed that the suitable annealing temperature to ensure the maximum reduction of oxygen groups is 600°C (Figure 4b). Authors also investigated the variation of  $sp^2$  to  $sp^3$  carbon ratio from fitting the C1s core level. They claimed a decrease of this ratio for increasing the annealing temperature up to 900°C. Due to artefacts linked to the nanometric size of NDs (Part 1.3), the  $CH_x$  contribution located at +0.5 eV from the diamond C1s core level well observed for boron doped diamond films after hydrogenation [69] cannot be detected for H-NDs. However, these C-H bonds were well evidenced by FTIR for both hydrogenation procedures [57, 66].

### ***Toward a selective oxidation of NDs***

Different oxidation treatments were developed to form specific oxygen functional groups at NDs surface. To generate carboxylic groups, oxidation of NDs was performed either by acid treatments [70] or by annealing under air at 400-430°C [71]. XPS was used to characterize HPHT NDs (10-15 nm) after acid treatment ( $H_2SO_4/HNO_3$ ) [72]. The fitting of the C1s core level showed the presence of C=O bonds with a peak up-shifted of 2.6 eV from the  $sp^3$  component after the oxidation. FTIR well confirmed the formation of carboxylic groups. Oxidized NDs were then suspended in water with a negative zeta potential of – 40 mV corresponding to the formation of carboxylate groups ( $COO^-$ ), the basic form of COOH, for pH > 5. After applying an acidic treatment, a Boehm titration ( $NaHCO_3$  in HCl) was successfully used to estimate the density of COOH groups present on detonation NDs to 0.85 sites per  $nm^2$  [73].

For detonation NDs annealed under air at 425°C, XPS revealed an increase of the oxygen content from 7 at % to 15 at. % with a decrease of the  $sp^2$  content at C1s core level [61]. These results were well confirmed by the evolution of the valence band. Initially, fingerprints of rings originating from the graphite shells present at NDs surface are detected while after oxidation, C2p related to  $\sigma$  bonds and O2p clearly appeared near 8 eV and 24 eV, respectively (Figure 5).

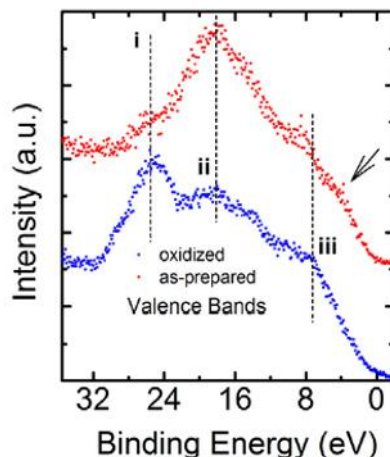


**Figure 5** Valence band of detonation nanodiamonds before and after air oxidation from [61]

Several procedures promoting hydroxylation were also reported. Compared to carboxylic groups which involve C=O bonds, hydroxyl groups based on C-O bonds induce a lower chemical shift at C1s core level ( $< 1$  eV). Due to artefacts previously underlined, the C1s is broadened for NDs with size smaller than 10 nm (Part 1.3). For this reason, XPS was less appropriate to characterize detonation NDs after hydroxylation. Lithium aluminium hydride or borane in THF were used to reduce carbonyl functions present at NDs surface [70]. FTIR characterization confirmed the vanishing of carbonyls and the formation of hydroxyls. A similar protocol based on  $\text{LiAlH}_4$  / THF was also applied to detonation NDs [74]. XPS, FTIR and NMR revealed very complementary techniques to characterize hydroxyls formation. For XPS, O1s core level was more sensitive to the surface modification than C1s one for nanodiamonds. Finally, the Fenton reaction was reported as another efficient method to generate OH groups at NDs surface as shown by FTIR [75]. Lastly, an ozone treatment under 150-200°C was applied to detonation NDs. XPS and NMR confirmed the reduction of  $\text{sp}^2$  carbon [76, 77]. In addition, the modified surface chemistry was characterized using Temperature Programmed Desorption (TPD) and FTIR.

### **Graphitization of NDs**

Annealing under vacuum can induce a progressive graphitization of NDs starting from their surface. According to their small size, the temperature threshold to initiate this mechanism is lowered compared to bulk diamond. A sequential approach of graphitization (annealing and XPS performed under UHV) will be presented in the Part 3 [78]. XPS was used after air exposure to characterize detonation NDs annealed at temperature included between 900°C and 1870°C [78]. The technique permits to quantify the increase of the  $\text{sp}^2$ -carbon peak downshifted from 1.3 eV toward the  $\text{sp}^3$ -carbon at the C1s core level. Moreover, for NDs annealed at 1330°C, the  $\pi$  plasmon located at + 5 eV from the  $\text{sp}^3$ -carbon was recorded. The study of the valence band showed the progressive rise of the  $\pi$  bonding fingerprint at 2.8 eV which becomes sharper with annealing temperature. A second structure related to  $\sigma$  bonding in graphite was simultaneously recorded. For higher temperature, a full graphitization led to the total transformation of NDs into Onion Like Carbon (OLCs). These XPS results were supported by HRTEM which showed the formation of several graphitic shells around NDs after annealing at 1330°C and OLCs for higher temperatures [79].

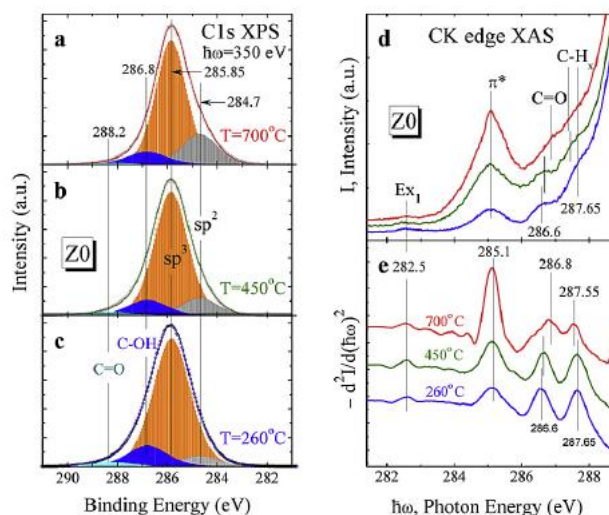


**Figure 6** C1s XPS spectra and CK edge XAS of NDs annealed at 260°C, 450°C and 700°C [80]

More recently, detonation NDs were annealed under vacuum at lower temperatures ranging from 260°C to 700°C. The goal was to initiate the early stages of graphitization to achieve the deaggregation of NDs. XPS showed the increase of the carbon  $sp^2$  component at C1s core level (Figure 6) [80]. X-ray Absorption Spectroscopy (XAS) investigations at C K edge allowed to confirm the formation of  $\pi^*$  bonds (Figure 6). TEM and Raman were also used to analyze these surface graphitized NDs.

### **Fluorination of NDs**

Annealing of detonation NDs under  $F_2/H_2$  atmosphere was reported at temperatures ranging from 150 to 470°C [62]. By XPS, a component located at + 1.9 eV towards  $sp^3$ -carbon was observed at C1s core level. It was assigned to fluorine covalently bonded to carbon. According to EDX analysis, the highest fluorine content is 8.6 at. % for the annealing at 470°C. A combined FTIR study confirmed C-F stretching bands. Another approach for HPHT NDs fluorination reported a radical substitution of carboxyls by fluorine using a reaction catalyzed by  $Ag^+$  [81]. The combined XPS analysis of F1s, C1s and O1s allowed to confirm the covalent attachment of fluorine on NDs. The C1s spectrum revealed different binding states of fluorine with carbon, with three contributions assigned to CF,  $CF_2$  and  $CF_3$  located at 2.1 eV, 6.5 eV and 9.2 eV from  $sp^3$  peak, respectively (Figure 7).

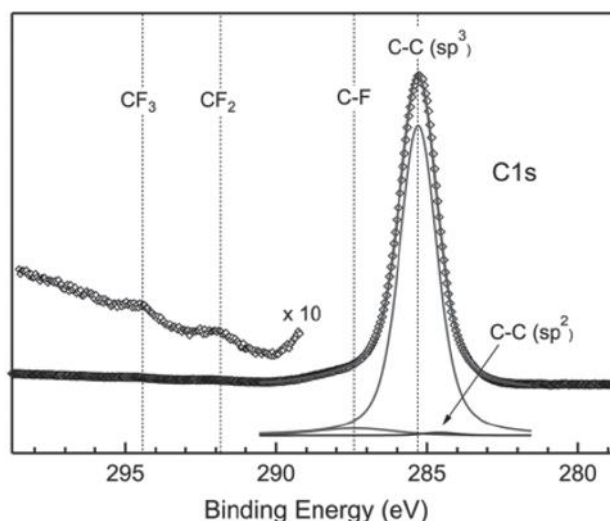


**Figure 7** C1s XPS spectra of fluorinated HPHT NDs [81]

### ***Combination of surface treatments***

The previous surface treatments have been also combined to improve the homogeneity of the surface chemistry or to achieve other surface terminations of NDs. As an illustration, few examples from the literature are discussed.

HPHT NDs first annealed under vacuum at 800°C were then oxidized under air at temperature ranging from 500°C to 600°C [82]. The aim was first to generate graphitic carbon at NDs surface and then to etch it efficiently under air exposure. The evolution of oxygen to carbon ratio was measured by XPS versus the annealing temperature. FTIR and Raman were combined to this study. In another report, surface graphitization of NDs was compared for as received and previously ozone-treated NDs [59]. Each kind of NDs was characterized by XPS before vacuum annealing. The atomic concentrations of carbon, oxygen and nitrogen were extracted. After annealing under vacuum at 750°C, more  $sp^2$ -carbon was present at the surface for pre-treated NDs according to Raman. TDMS showed a higher oxygen concentration on these NDs and more carbonyl and carboxylic acid anhydride functional groups. After a multi-step protocol starting from hydroxylated NDs, amino groups were formed at detonation NDs [83]. FTIR showed the presence of N-H groups at the surface. The evolution of the N1s core level indicated an increase of nitrogen atoms bonded to  $sp^3$  carbon which is consistent with the formation of  $NH_2$  groups at the surface. Lastly, plasma hydrogenated HPHT NDs were exposed to UV under water vapor atmosphere [84]. The formation of hydroxyl groups was evidenced by a combination of XPS and FTIR analyses. A density of one OH group per nm was extracted from the data. Lastly, amino groups were produced on detonation NDs in three successive steps: an acid treatment to form carboxylic groups, a chlorination under Oxalyl Chloride in THF, an amination in THF under dry  $NH_3$  [85]. XPS allowed to show the presence of chlorine after the second step and the enrichment in nitrogen after the amination (Figure 8).

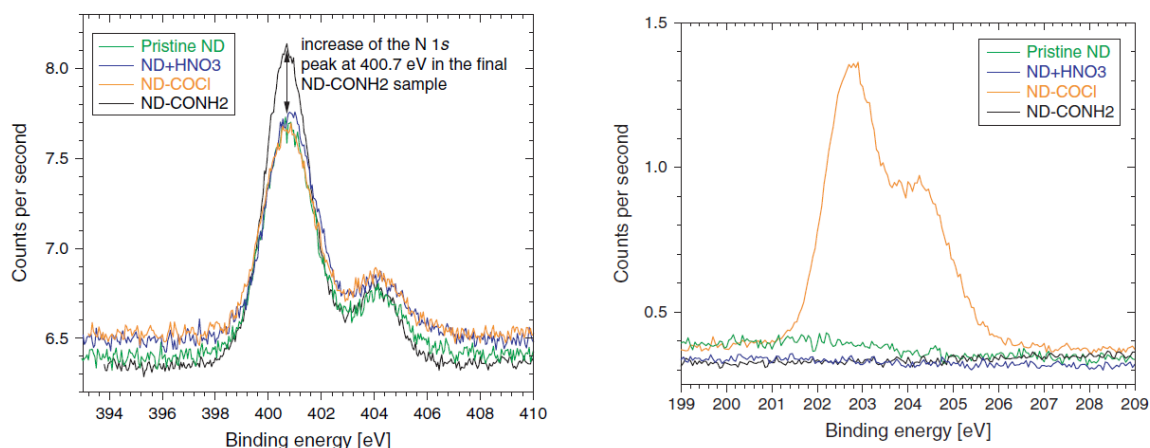


**Figure 8** N1s (left) and Cl2p (right) recorded after each step used for amination of NDs [85]

### 2.3 Functionalized NDs

Due to the versatile carbon chemistry, NDs could be functionalized with more complex molecules like biomolecules, proteins or polymers. Such molecule attachment could be achieved either by electrostatic interactions [86] or by creation of covalent bonds [87]. More often, such grafting implies multi-steps starting from surface modified NDs (Part 2.2). XPS revealed a powerful surface analysis to validate intermediate steps. As an illustration, the immobilization of proteins was demonstrated on fluorescent HPHT NDs containing nitrogen-vacancy color centers from a preliminary grafting of nitrophenyl groups [88]. In this study, the functionalization of nitrophenyl groups onto HPHT NDs was carried out in water via the reduction of aryl diazonium salts under ultrasounds [89]. XPS allowed to detect the  $\text{NO}_2$  terminations of the phenyl groups which led to an additional component at N1s core level located at + 6 eV compared to the one corresponding to nitrogen included in HPHT NDs. At C1s, the proximity of contributions originating from C-N and C-O bonds located at + 0.8 eV and + 1.5 eV from  $\text{sp}^3$ -carbon, respectively, complicates the analysis. The amount of  $\text{NO}_2$  was deduced from XPS data for different grafting conditions. A FTIR study completed this work. An alternative diazonium grafting was applied to HPHT NDs previously hydrogenated. In this case, the electron exchange can arise thanks to the SCL of hydrogenated diamond surface [84]. XPS revealed the presence of  $\text{sp}^2$  carbon assigned to phenyl groups at carbon core level while  $\text{NO}_2$  groups were identified from the N1s core level. The bovine serum albumine (BSA) was bonded to HPHT NDs grafted with brominated aryl diazonium groups followed by a polymerization of tert-butyl methacrylate (tBMA) and a coupling with BSA [88]. The XPS analysis of Br3d, C1s and O1s core levels permits a monitoring of the polymerization versus time with an estimation of the polymer thickness extracted from data. As stated previously, FTIR revealed very complementary to XPS to characterize the grafting.

A second example concerns the grafting of monomer polyethylene glycol (PEG) chains onto detonation NDs to enhance their solubility in biologic media [90]. The goal is to get highly furtive NDs for bioapplications. For this purpose, three steps were achieved: first, NDs were oxidized via acid treatment to favor carboxyl functional groups at their surface. Then, carboxylic groups reacted with thionyl chloride to form acyl chloride groups. PEG chains were grafted by an esterification reaction of COOH from NDs with OH group at PEG chains (Figure 9). Polymer grafted ratio extracted from XPS was found in agreement with the one measured by TGA. This study also

presented an alternative grafting of poly(ethylene glycol)methyl ether methacrylate (PEGMA) through NDs behaving Br terminations [90]. XPS was used to evidence the Br termination.

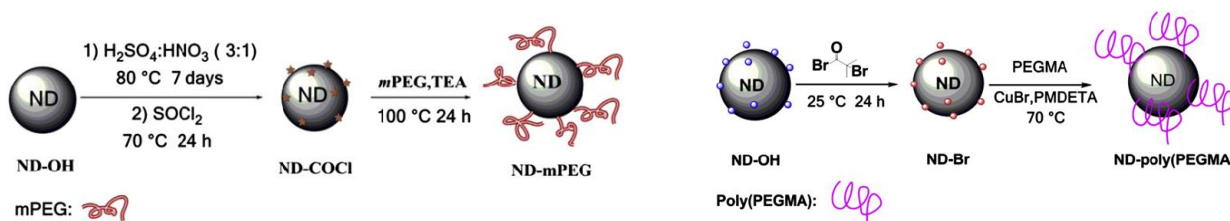


**Figure 9** Representations of PEG and PEGMA coatings of NDs [90]

### 3. XPS to investigate the reactivity of NDs under different atmospheres

In the previous parts, the XPS technique was used as an analytical tool in combination with other techniques to characterize the changes in surface chemistry of NDs after different surface treatments (Parts 2.2 and 2.3). Samples were exposed to air before the XPS characterization. The present paragraph will focus on few studies which used XPS to monitor surface modifications induced by plasma or thermal treatments performed *in vacuo*, samples being analyzed without air exposure. This sequential approach allowed to investigate the reactivity of NDs in different atmospheres without contamination of samples.

#### 3.1 Monitoring the surface modifications of nanodiamonds

##### **Hydrogenation**

As previously underlined, hydrogen termination is an efficient way to get a homogeneous surface chemistry for NDs (Part 2.2). Surface graphitized detonation NDs were exposed to atomic hydrogen produced by thermal cracking of hydrogen molecules at  $10^{-9}$  mbar [91]. XPS performed with synchrotron facilities revealed the removal of  $sp^2$  carbon after exposure to atomic hydrogen at C1s core level. This was confirmed by the valence band spectra with the vanishing of the  $\pi$  structure and the presence of the  $sp^3 \sigma$  (Figure 10b). An up-shift of the  $sp^3$  C1s component of 0.9 eV is observed for hydrogenated NDs compared to the graphitized one. It is assigned to band bending. If hydrogenated NDs are annealed under vacuum at 930°C, graphitic external shells are formed and the  $sp^2$  signature is recovered in valence band spectra (Figure 10d).

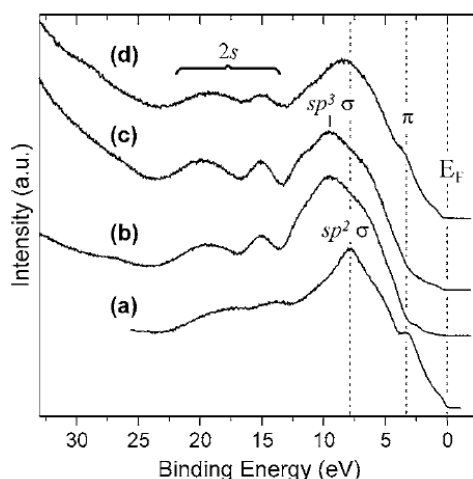


**Figure 10** Valence band spectra recorded with photons of 55 eV: (a) as received NDs; (b) exposed to atomic hydrogen; (c) vacuum annealed at 730°C; (d) vacuum annealed at 930°C [91]

The modifications of the electronic structure of detonation NDs exposed to atomic hydrogen ( $10^{-6}$  mbar) produced by a hot filament were also monitored by XPS, XEELS and XAES [92]. The estimated temperature of NDs under hydrogen exposure was 430°C. Contrary to the graphite reference, NDs didn't exhibit the  $\pi$  peak in the XEELS spectrum which looks very similar to diamond. Nevertheless, the  $\pi$  contribution is detected in the XAES C KVV transition because XAES probes the first upper planes. Belobrov et al. concluded about the presence of surface states ( $\sigma_s^1 \sigma_p^2 \pi^1$ ) without overlapping of  $\pi$  levels.

Plasma hydrogenation of detonation NDs seeded on a substrate was investigated by XPS and AES using a UHV set-up connected to a Microwave Plasma CVD reactor [93]. Plasma parameters were tuned corresponding to sample temperatures ranging from 520°C to 860°C. After the plasma exposure, the reactor was pumped down to a pressure of  $7 \times 10^{-7}$  mbar. A sequential XPS analysis of surface effects of hydrogen MPCVD plasma was thus carried out. A plasma exposure at 700°C is required to remove oxygen functional groups at NDs surface, no more oxygen is detected on XPS spectra. If a higher sample temperature is reached under hydrogen plasma (860°C), an up-shift of 0.8-1 eV is observed at C1s core level. This result is in agreement with the one reported previously for NDs exposed to atomic hydrogen [91]. The origin of this upshift is attributed to the non-conductive surface of hydrogenated diamond. The kinetics of oxygen desorption has been also investigated for plasma conditions corresponding to 520°C. XPS results showed only a partial removal of oxygen functional groups at this temperature even after 2h of annealing. This temperature is insufficient to break a part of carbon/oxygen bonds. The ageing at ambient air of NDs hydrogenated at 700°C was studied. A strong adsorption of molecules was evidenced by XPS (Figure 11a). This study demonstrated the reactivity of hydrogenated NDs towards ambient air. In situ thermal treatments were then performed to remove adsorbed oxygen functional groups (Figure 11b and c). This sequential investigation allowed to define the proper parameters for plasma hydrogenation. A set-up devoted to plasma hydrogenation of NDs powder was further developed [57].



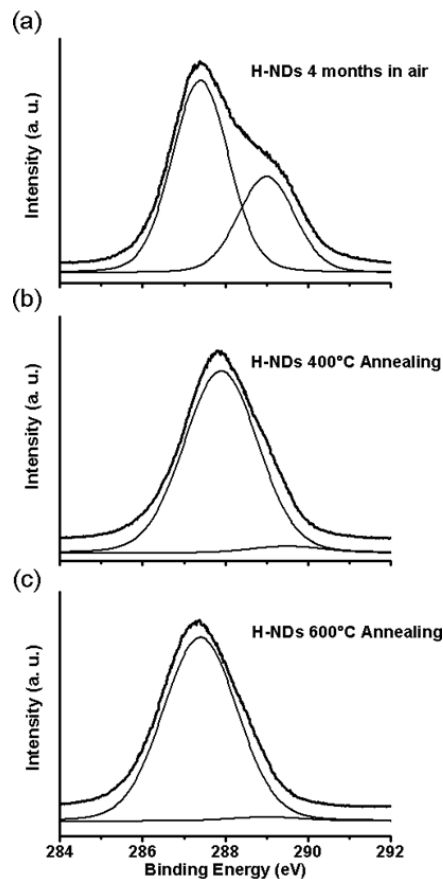


**Figure 11** Evolution of C1s core level for plasma H-NDs (a) exposed to air ; (b) annealed at 400°C under UHV; (c) annealed at 600°C under UHV [93]

### ***Annealing or plasma exposure of NDs seeded on surfaces***

Nanodiamonds are commonly used as seeds for growth of thin diamond films on various substrates [94]. The knowledge of the reactivity of NDs under CVD plasma conditions provides important information on the nature of the diamond/substrate interface. Sequential XPS studies have been carried out on silicon and silicon nitride substrates seeded with detonation NDs.

Hydrogen MPCVD plasma was applied to detonation NDs seeded onto silicon substrate [95]. A sequential *in situ* XPS analysis performed in a UHV set-up connected to the MPCVD reactor allowed to investigate the interactions between hydrogen species from the plasma and NDs. Two different plasma conditions were applied corresponding to 720°C and 940°C for two durations 15 and 45 minutes. Whatever the hydrogen plasma, NDs seeds are preserved at the surface and revealed after a short growth under CH<sub>4</sub>/H<sub>2</sub> CVD plasma.

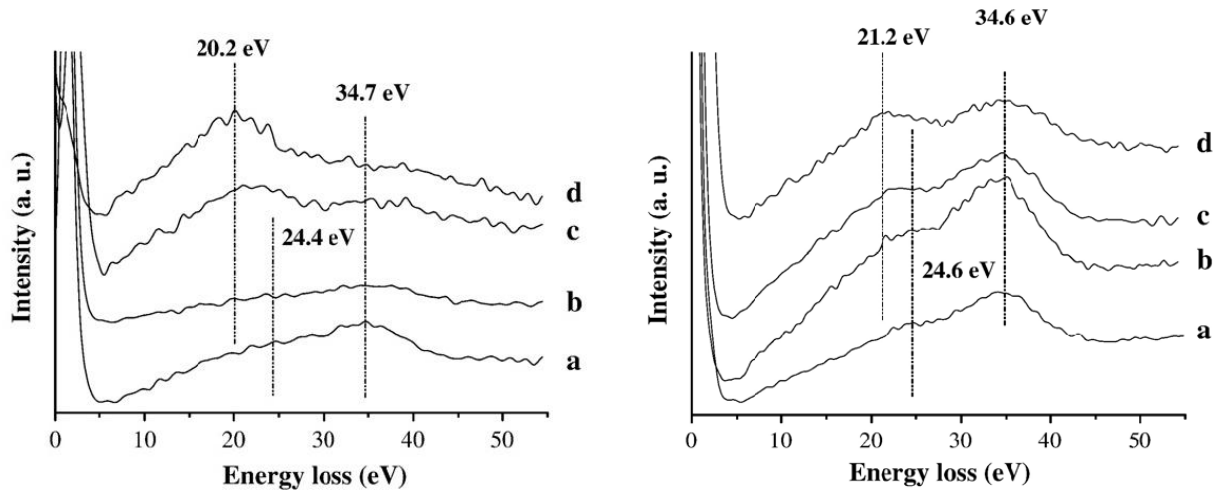


**Figure 12** XEELS spectra (left) after H<sub>2</sub> plasma; (right) after H<sub>2</sub> plasma and a short CVD growth (a) as introduced; (b) after a H<sub>2</sub> plasma at 720°C/15 min; (c) after a H<sub>2</sub> plasma at 940°C/15 min; (d) after a H<sub>2</sub> plasma at 940°C/45 min [95]

The formation of a silicon carbide interlayer is evidenced by XEELS spectra after the H<sub>2</sub> plasma (Figure 12 left). Indeed, in addition to the surface and bulk plasmons assigned to diamond located at 24.4 eV and 34.7 eV, respectively, the one related to silicon carbide appears to 20.2 eV. The silicon carbide signature was also found at C1s and Si2p core levels. XEELS recorded after the short CVD growth well evidenced the formation of diamond crystals (Figure 12 right).

Under CVD plasma, both thermal and chemical mechanisms are involved. To better understand the thermal stability of NDs seeded on silicon substrates, UHV annealing was applied to NDs at different temperatures [96]. After thermal treatment at 800°C, NDs were preserved with a comparable density versus non annealed sample as shown by XPS and SEM analyses after a short growth step.

On the contrary, at 900°C, no diamond signal was detected suggesting a transformation of NDs. After the UHV treatment at 900°C, the Si 2p core level (Figure 13c) and XEELS spectra showed the signature of silicon carbide at the surface. This silicon carbide was not observed after the annealing at 800°C. It is interesting to remark that the thermal stability of NDs is worse than the one under plasma. Indeed, the previous study underlined stability of NDs up to 940°C. This was attributed to the possible passivation of diamond surface by atomic hydrogen from the plasma.

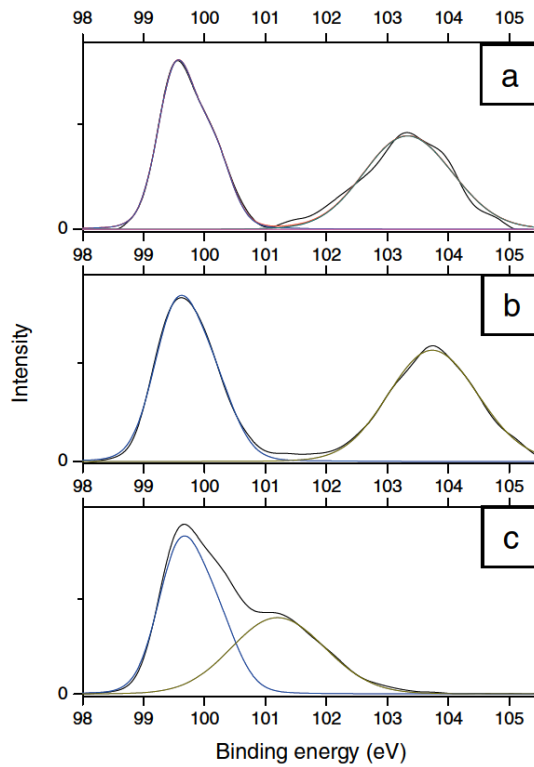


**Figure 13** Si2p spectra (a) as introduced (b) after annealing at 800°C (c) after H<sub>2</sub> plasma at 900°C [96]

To avoid the interdiffusion between NDs and silicon, a similar study was reported on NDs seeded on silicon nitride overlayer [97]. The goal was to assess the intrinsic thermal stability of NDs. The temperature was varied within the range 400-1050°C. The *in situ* XPS analysis allowed to show the evolution of carbon, oxygen, silicon and nitrogen atomic concentrations versus the annealing temperature (Figure 14).

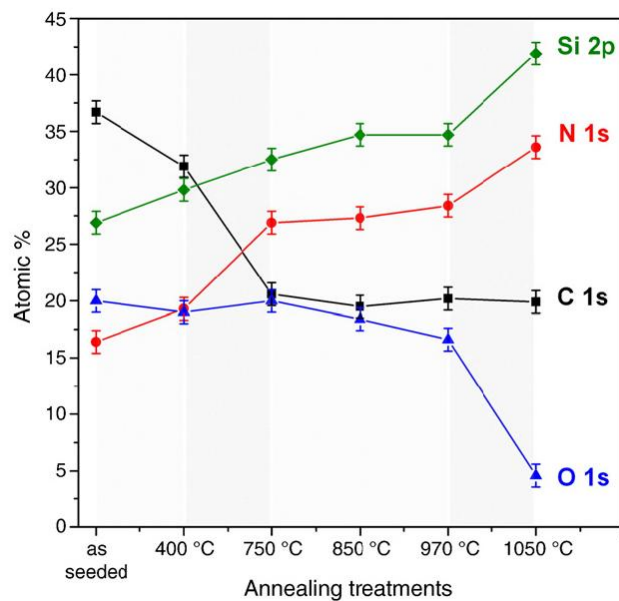


**Figure 14** Evolution of silicon, nitrogen, carbon and oxygen atomic concentrations versus the annealing temperature [97]

The oxygen concentration started to decrease at 850°C while it dropped at 1050°C (Figure 14). The detailed analysis of the C1s core level showed that hydroxyl and ether groups were desorbed first. At 1050°C, C=O bonds are broken. NDs were found to be stable up to 1050°C, a short CVD growth step leading to a diamond film close to full surface coverage according to SEM. No complete transformation of NDs into carbon onions was observed even after the annealing at 1050°C. However, for this temperature range, the graphitization of the diamond core of NDs has started (Part 3.1). In this study, XPS and XEELS spectra were used to investigate the kinetics of desorption of oxygen groups and the thermal stability of NDs.

### Surface graphitization

Using the same sequential approach, the early stages of surface graphitization of detonation NDs were studied by XPS after annealing under UHV [78]. The evolution of the C1s core level allowed to monitor the formation of  $sp^2$  carbon at NDs surface for different temperatures and durations (Figure 15). At 700°C, only a weak  $sp^2$  contribution is detected by XPS. The  $sp^2$  contribution raised with the temperature and annealing time. XPS allowed to show that the  $sp^3$  core of NDs started to graphitize at 1100°C with a decrease of the  $sp^3$  component at C1s. Below 900°C, graphitic reconstructions (fullerene like reconstructions [98]) are formed at NDs surface whereas for higher temperature, several graphitic outershells are induced as shown by high resolution TEM studies [78-79]. This XPS study was well correlated with the one of Liang et al. who investigated the chemical reactivity of NDs annealed at 750°C to initiate arylation reactions [99]. NDs treated at lower temperature didn't exhibit this chemical reactivity.

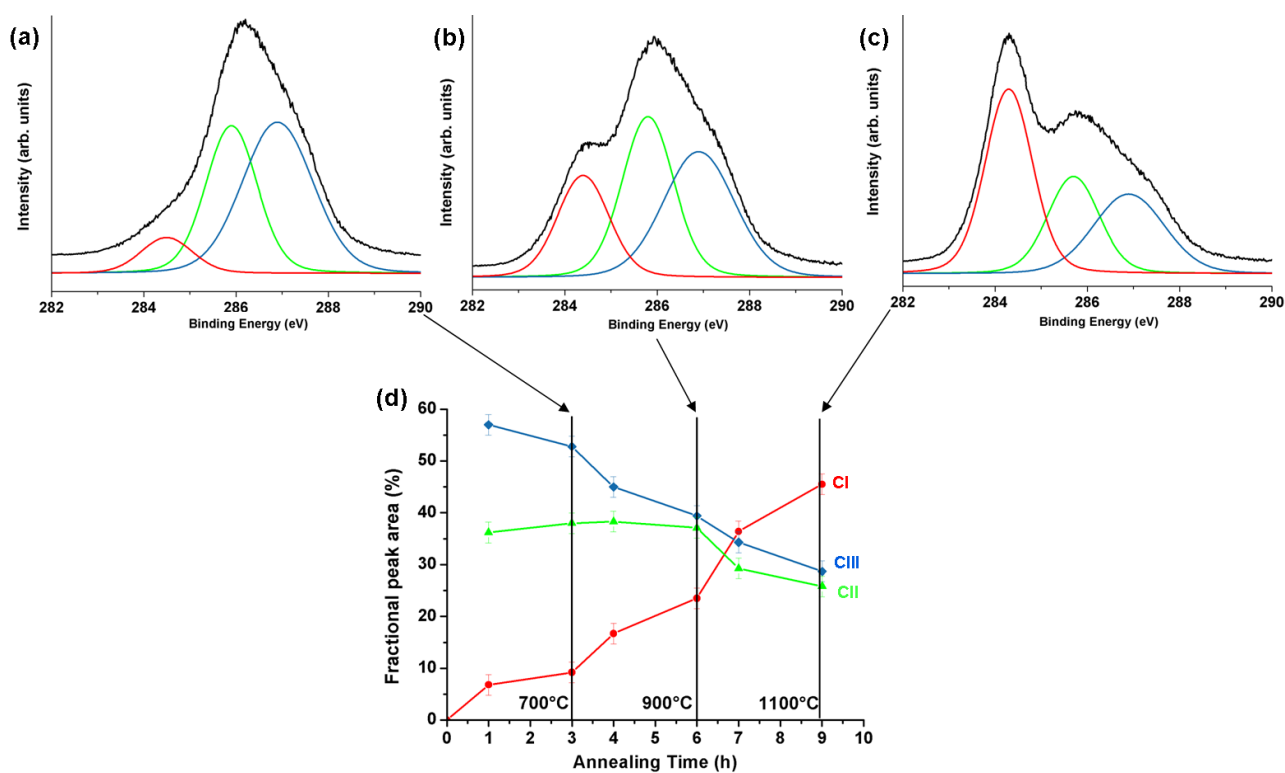


**Figure 15** Evolution of C1s core level for different annealing temperatures and annealing times, C1, CII and CIII correspond to  $sp^2$  carbon,  $sp^3$  carbon and defects, respectively [78].

NDs were annealed under UHV at higher temperatures to reach a complete transformation into onion like carbons (OLC) [100]. OLC were then evaporated onto silicon substrates. XPS performed in situ revealed the signature of graphite at C1s core level. Raman spectroscopy confirmed the presence of the D and G bands characteristics of graphitic materials and HRTEM showed the OLC structure.

These sequential XPS studies were essential to investigate the kinetics of graphitization of NDs and to adjust the graphitization stages from  $sp^2$  reconstructed NDs to OLC.

### 3.2 Monitoring the reactivity of NDs

#### *Hydrogenated NDs from aqueous colloidal suspension*

Plasma H-NDs behaves a negative electron affinity (NEA) as shown by STS measurements [68]. To investigate the reactivity of H-NDs towards water molecules, H-NDs stable in water were dried and characterized by XPS [7]. The oxygen atomic concentration measured by XPS was 3 at. % corresponding to an adsorption of water molecules. An *in situ* annealing at 400°C led to the drop of oxygen down to 1 at. %. At the same time, the C1s peak underwent an up-shift in binding energy of 1 eV (Figure 16). This upshift corresponds to the removal of the main part of adsorbates from hydrogenated diamond surface. These experiments confirmed the formation of a surface conductive layer (SCL) on H-NDs which were exposed to water. The presence of a SCL was previously demonstrated for hydrogenated surfaces of bulk diamond exhibiting different crystallographic orientations [12, 101, 102]. XPS allowed to monitor the removal of adsorbates by in situ annealing.

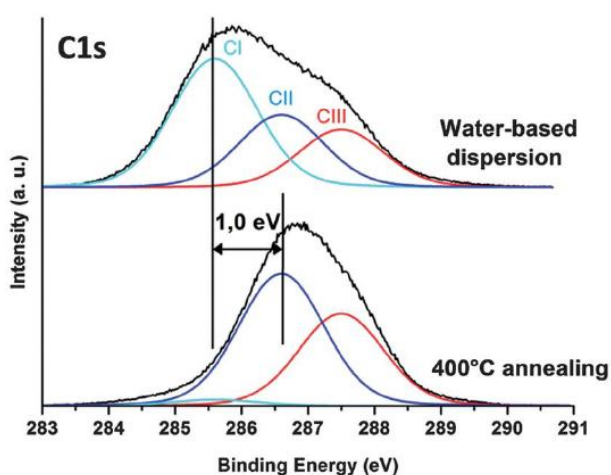


**Figure 16** C1s core level of dried H-NDs from aqueous suspension (top) and after in situ annealing at 400°C (down). CI is related to a surface conductive layer formed on H-NDs after air exposure while CII and CIII are assigned to  $sp^3$  carbon bonds from the diamond core and structural defects and C-N bonds, respectively. [7]

## Conclusion and Perspectives

The surface chemistry strongly governs the properties of nanodiamonds. X-ray Photoemission Spectroscopy (XPS) is a technique of choice to characterize this surface chemistry either after modifications of surface terminations or after a grafting procedure. For NDs of small size (< 10 nm), artefacts affecting photoemission peaks should be taken into account (Part 1.3). In the literature, XPS is usually combined with other techniques like FTIR, NRM, TDMS, Raman or HRTEM to fully characterize the surface chemistry and the crystalline structure of NDs. Indeed, these techniques offer different probed depths, limits of detection and detected elements (Table 2). A special attention should be taken for the deposition of NDs on substrates for XPS analysis to limit the charging effects.

The present paper reviewed the main XPS inputs to characterize NDs after surface modifications like hydrogenation, oxidation, graphitization or fluorination (Part 2.1). Several examples were provided to illustrate the role of XPS in the analysis of functionalized NDs via multi-step protocols (Part 2.2).

Most importantly, *in situ* sequential XPS permits to investigate the surface reactivity or the stability of NDs toward different atmospheres like ambient air, CVD plasma or UHV annealing. The analysis of core levels in XPS can be correlated with XEELS spectra while the valence band can be probed either using synchrotron or by UPS. In addition, X-ray excited C KVV Auger transitions are very complementary to XPS which gives access to the chemical shift while XAES contains the convolution of  $\pi$  and  $\pi$ - $\sigma$  states in the valence band. The combination of these surface analyses revealed fruitful to better understand the stability of NDs under plasma or annealing treatments. According to the recent report of Fujimoto et al. [48] on 1  $\mu$ m diamond particles embedded in HOPG, the charging effects on the position of  $sp^2$  and  $sp^3$  carbon must be better understood and taken into account in the XPS C1s spectra of nanodiamonds.

More recently, new techniques based on X-rays emerged, like X-ray emission (XES) and absorption (XAS) spectroscopies revealed powerful to investigate interactions between NDs and solvent in colloidal suspensions by probing carbon and oxygen K edges [103]. In particular, modifications in the structure of water molecules surrounding NDs were measured for various surface chemistry from hydrogenated to carboxylated and hydroxylated detonation NDs [104]. With the last progresses of XPS instrumentation, set-ups are now able to operate at ambient pressure [105]. Using synchrotron facilities, XPS analysis can be performed on isolated nanoparticles. This technique was previously used to investigate the photoreactivity of TiO<sub>2</sub> nanoparticles toward water molecules [106]. These new experimental tools open the way for a deeper understanding of interactions between NDs and solvents. This knowledge is required to achieve a higher control of stable colloidal suspensions for applications in biology or energy.

## Acknowledgements

J. C. Arnault would like to thank his colleagues involved in XPS studies of NDs: H. A. Girard, T. Petit, A. Venerosy, C. Gesset, S. Saada, S. Zeppilli and R. Polini (Tor Vergata University, Rome). J. C.

Arnault also acknowledges Prof. Dr. Anke Krueger (Würzburg University) for giving the opportunity to present this review work.

## References

- [1] O. A. Shenderova, N. Nunn, Production and purification of nanodiamonds in: *Nanodiamonds Advanced Material Analysis, Properties and Applications*, J. C. Arnault Ed. (Elsevier (2017) pp 25-56.
- [2] A. Krueger, D. Lang, Functionality is Key: Recent Progress in the Surface Modification of Nanodiamond, *Adv. Funct. Mater.* 22 (2012) pp 890-906.
- [3] O. A. Shenderova, G. E. McGuire, Science and engineering of nanodiamond particle surfaces for biological applications, *Biointerphases* 10 (2015) 030802 1-23.
- [4] K. Turcheniuk and V. N. Mochalin, Biomedical applications of nanodiamond, *Nanotechnology* 28 (2017) 252001
- [5] I. Neitzel, V. N. Mochalin, Y. Gogotsi, Nanodiamonds in composites: polymer chemistry and tribology in: *Nanodiamonds Advanced Material Analysis, Properties and Applications*, J. C. Arnault Ed. (Elsevier (2017) pp 365-395.
- [6] M. Ivanov, O. A. Shenderova, Nanodiamond-based nanolubricants for motor oils, *Current Opinion in Solid State and Materials Science* (2016)
- [7] T. Petit, H. A. Girard, A. Trouvé, I. Batonneau-Gener, P. Bergonzo, J. C. Arnault, Surface transfer doping can mediate both colloidal stability and self-assembly of nanodiamonds, *Nanoscale* 5 (2013) pp 8958-8962.
- [8] T. Petit, J. C. Arnault, H. A. Girard, M. Sennour, T. Y. Kang, C. L. Cheng, P. Bergonzo, Oxygen hole doping of nanodiamond, *Nanoscale* 4 (2012) pp 6792-6799.
- [9] R. Grall, H. A. Girard, L. Saad, T. Petit, C. Gesset, M. Combis-Schlumberger, V. Paget, J. Delic, J. C. Arnault, S. Chevillard, Impairing the radioresistance of cancer cells by hydrogenated Nanodiamonds, *Biomaterials* 61 (2015) 290-298.
- [10] M. Kurzyp, H. A. Girard, Y. Cheref, E. Brun, C. Sicard-Roselli, S. Saada, J. C. Arnault, Hydroxyl radical production induced by plasma hydrogenated nanodiamonds under X-ray irradiation, *Chem. Comm.* (2017).
- [11] L. Ley, R. Graupner, J.B. Cui, J. Ristein, Electronic properties of single crystalline diamond surfaces, *Carbon* 37 (1999) pp 793–799.
- [12] J. Ristein, Surface science of diamond: Familiar and amazing, *Surf. Science* 600 (2006) pp 3677–3689.
- [13] H. Hertz, Ueber sehr schnelle elektrische Schwingungen, *Ann. Physik* 31,983 (1887).
- [14] M. P. Seah, in *Practical surface Analysis (Second Edition)*, ed. D. Briggs and M. P. Seah, Wiley and Sons, Chichester, England, 1993.
- [15] P. Van der Heide, *XPS Instrumentation in “X-Ray Photoelectron Spectroscopy: An Introduction to Principles and Practices”*, John Wiley & Sons (2011) DOI: 10.1002/9781118162897.ch3

- [16] P. J. Cumpson (2003) In: Briggs D, Grant JT (eds) Surface analysis by Auger and X-ray photoelectron spectroscopy, IMPublications, Chichester, pp 651–675
- [17] P Weightman, X-ray-excited Auger and photoelectron spectroscopy, Rep. Prog. Phys. 45 (1982) 753-815
- [18] F. Rochet, H. Roulet, G. Dufour, S. Carniato, C. Guillot, N. Barrett, M. Froment, Si(001) vicinal surface oxidation in O<sub>2</sub>: angle-resolved Si 2p core-level study using synchrotron radiation, Appl. Surf. Sci. 59 (1992) p 117-134.
- [19] C. S. Fadley, X-ray photoelectron spectroscopy: Progress and perspectives, J. Electron Spectroscopy and Related Phenomena 178-179 (2010) p 2-32.
- [20] A. Shchukarev, XPS at solid–aqueous solution interface, Advances in Colloid and Interface Science 122 (2006) 149–157
- [21] H. Sezen, S. Suzer, XPS for chemical- and charge-sensitive analyses, Thin Solid Films 534 (2013) 1–11
- [22] J. H. Scofield, Hartree-Slater subshell photoionization cross-sections at 1254 and 1487 eV, J. Elect. Spect. Relat. Phenomena 8 (1976) pp 129-137.
- [23] J.C. Arnault, S. Saada, S. Delclos, L. Intiso, N. Tranchant, R. Polini, P. Bergonzo, In situ study of the initial stages of diamond deposition on 3C–SiC (100) surfaces: Towards the mechanisms of diamond nucleation, Diam. Relat. Mater. 16 (2007) pp 690-694.
- [24] C. Agnes, J. C. Arnault, F. Omnes, B. Jusselme, M. Billon, G. Bidan, P. Mailley, XPS study of ruthenium tris-bipyridine electrografted from diazonium salt derivative on microcrystalline boron doped diamond, Phys. Chem. Chem. Phys. 11 (2009) pp 11647-11654.
- [25] S. Tanuma, C.J. Powell, D.R. Penn, Calculations of electron inelastic mean free paths, Surf. Interface Anal. 17 (1991) pp 911
- [26] P. S. Bagus, E. S. Ilton, C. J. Nelin, The interpretation of XPS spectra: Insights into materials properties, Surf. Sci. Reports 68 (2013) 273-304
- [27] J. Cazaux, Mechanisms of charging in electron spectroscopy, J. Electron. Spectrosc. Relat. Phenom. 105 (1999) 155.
- [28] A. Jablonski, Elastic scattering and quantification in AES and XPS, Surf. Interf. Analysis 14 (1989) 659-685.
- [29] S. Tougaard, Energy loss in XPS: Fundamental processes and applications for quantification, non-destructive depth profiling and 3D imaging, J. Elect. Spect. Relat. Phenomena 178-179 (2010) p 128-153.
- [30] D. G. F. David, M. A. Pinault-Thaury, D. Ballutaud, C. Godet, Sensitivity of photoelectron energy loss spectroscopy to surface reconstruction of microcrystalline diamond films, Appl. Surf. Sci. 273 (2013) p 607-612.
- [31] J. C. Lascovich, R. Giorgi, S. Scaglione, Evaluation of the sp<sup>2</sup>/sp<sup>3</sup> ratio in amorphous carbon structure by XPS and XAES, Appl. Surf. Science 47 (1991) p 17-21.



- [32] Y. Mizokawa, T. Miyasato, S. Nakamura, K. M. Geib, C. W. Wilmsen, Comparison of the KLL first derivative Auger spectra from XPS and AES using diamond, graphite, SiC and diamond-like-carbon films, *Surf. Science* 182 (1987) pp 431-438.
- [33] S. Kaciulis, A. Mezzi, P. Calvani, D. M. Trucchi, Electron spectroscopy of the main allotropes of carbon, *Surf. Interf. Anal.* 46 (2014) p 966-969.
- [34] C. Benndorf, S. Hadenfeldt, W. Luithardt, A. Zhukov, Photoelectron spectroscopic investigations and exoelectron emission of CVD diamond surfaces modified with oxygen and potassium, *Diam. Relat. Mater.* 5 (1996) p 784-789.
- [35] L. Diederich, O.M. Küttel, P. Aebi, L. Schlapbach, Electron affinity and work function of differently oriented and doped diamond surfaces determined by photoelectron spectroscopy, *Surf. Sci.* 418 (1998) p 219-239.
- [36] S. Michealson and A. Hoffman, HR-EELS investigations of hydrogenated nanodiamond films in "Nanodiamonds, Advanced Material Analysis, Properties and Applications" Ed J.C. Arnault (Elsevier, 2017).
- [37] G. A. Inel, E. M. Ungureau, T. S. Varley, M. Hirani, K. B. Holt, Solvent–surface interactions between nanodiamond and ethanol studied with in situ infrared spectroscopy, *Diam. Relat. Mater.* 61 (2016) p 7-13.
- [38] L. A. McDonnell, R. M. A. Heeren, Imaging mass spectrometry, *Mass Spectr. Rev.* 26 (2007) p 606-643.
- [39] A. R. Krylov, E. V. Lychagin, A. Yu. Muzychka V. V. Nesvizhevsky, G. V. Nekhaev, A. V. Strelkov, A. S. Ivanov, Study of bound hydrogen in powders of diamond nanoparticles, *Crystall. Reports* 56 (2011) p 1186-1191.
- [40] P. N. Nesterenko, D. Mitev, B. Paull, Elemental analysis of nanodiamonds by inductively coupled plasma hyphenated methods in "Nanodiamonds, Advanced Material Analysis, Properties and Applications" Ed J.C. Arnault (Elsevier, 2017).
- [41] S. Ghodbane, D. Ballutaud, F. Omnès, C. Agnès, Comparison of the XPS spectra from homoepitaxial {111}, {100} and polycrystalline boron-doped diamond films, *Diam. Relat. Mater.* 19 (2010) p 630-636.
- [42] A. P. Koscheev, Gas desorption from detonation nanodiamonds during temperature-programmed pyrolysis, *Carbon Nanomaterials for Gas Adsorption* (2012) pp 219-252.
- [43] M. Dubois, K. Guerin, E. Petit, N. Batische, A. Hamwi, N. Komatsu, J. Giraudet, P. Pirotte, F. Masin, Solid-State NMR Study of Nanodiamonds Produced by the Detonation Technique, *J. Phys. Chem. C* 113 (2009) pp 10371-10378.
- [44] K.P. Loh, X.N. Xie, Y.H. Lim, E.J. Teo, J.C. Zheng, T. Ando, Surface oxygenation studies on (100)-oriented diamond using an atom beam source and local anodic oxidation, *Surf. Sci.* 505 (2002) pp 93-114.
- [45] B. Zhang, B. Yan, Analytical strategies for characterizing the surface chemistry of nanoparticles, *Anal. Bioanal. Chem.* 396 (2010) pp 973-982.
- [46] C. Mer-Calfati, N. Tranchant, P. N. Volpe, F. Jomard, S. Weber, P. Bergonzo, J. C. Arnault, Sharp interfaces for diamond delta-doping and SIMS profile modelling, *Mater. Lett.* 115 (2014) 283-286.

- [47] S. Hajati, S. Tougaard, XPS for non-destructive depth profiling and 3D imaging of surface nanostructures, *Anal Bioanal Chem* 396 (2010) 2741–2755
- [48] A. Fujimoto, Y. Yamada, M. Koinuma, S. Sato, Origins of  $sp^3C$  peaks in C1s X-ray Photoelectron Spectra of Carbon Materials, *Anal. Chem.* 88 (2016) pp 6110-6114.
- [49] S. Hajati, S. Coultas, C. Blornfield, S. Tougaard, Nondestructive quantitative XPS imaging of depth distribution of atoms on the nanoscale, *Surface and Interface Analysis* 40 (2008) pp 688–691.
- [50] D. R. Baer, M. H. Engelhard, XPS analysis of nanostructured materials and biological surfaces, *J. Elect. Spectr. Relat. Phenom.* 178-179 (2010) pp 415-432.
- [51] Y. C. Wang, M. H. Engelhard, D. R. Baer, D. G. Castner, Quantifying the Impact of Nanoparticle Coatings and Nonuniformities on XPS Analysis: Gold/Silver Core–Shell Nanoparticles, *Anal. Chem.* 88 (2016) pp 3917-3925.
- [52] D.-Q. Yang, E. Sacher, Initial and final state effects on metal/cluster/substrate interactions, as determined by XPS: copper clusters on dodecylbenzene and highly oriented pyrolytic graphite, *Applied Surface Science* 195 (2002) 187–195.
- [53] M. Y. Smirnov, A. V. Kalinkin, A. V. Bukhtiyarov, I. P. Prosvirin, V. I. Bukhtiyarov, Using X-ray Photoelectron Spectroscopy To Evaluate Size of Metal Nanoparticles in the Model Au/C Samples, *J. Chem. Phys. C* 102 (2016) pp 10419-10426.
- [54] J.A. Smith, M. Josowicz, M. Engelhard, D.R. Baer, J. Janata, Gold-polyaniline composites, *Physical Chemistry Chemical Physics* 7 (20) (2005) 3619–3625.
- [55] D. R. Baer, M. H. Engelhard, G. E. Johnson, J. Laskin, J. Lai, K. Mueller, P. Munusamy, S. Thevuthasan, H. Wang, N. Washton, A. Elder, B. L. Baisch, A. Karakoti, S. V. N. T. Kuchibhatla, D. Moon, Surface characterization of nanomaterials and nanoparticles: Important needs and challenging opportunities, *J. Vac. Sci. Technol. A* 31(2013) 050820 1-34
- [56] J. C. Arnault, *Nanodiamonds: From Synthesis and Purification to Deposition Techniques, Hybrids Fabrication and Applications in Carbon Nanoparticles and Nanostructures*, N. Yang et al. (Eds) Springer 2016.
- [57] H. A. Girard, J. C. Arnault, S. Perruchas, S. Saada, T. Gacoin, J. P. Boilot, P. Bergonzo, Hydrogenation of nanodiamonds using MPCVD: A new route toward organic functionalization, *Diam. Relat. Mater.* 19 (2010) pp 1117-1123.
- [58] S. Su, J. Li, V. Kundrat, A. M. Abbot, H. Ye, Hydrogen-terminated detonation nanodiamond: Impedance spectroscopy and thermal stability studies, *J. Appl. Phys.* 113 (2013) 023707 1-8.
- [59] J. C. Arnault, T. Petit, H. A. Girard, C. Gesset, M. Combis-Schlumberger, M. Sennour, A. Koscheev, A. A. Khomich, I. Vlasov, O. Shenderova, Surface graphitization of ozone treated detonation nanodiamond, *Phys. Stat. Sol. A* 211 (2014) p 2739-2743.
- [60] C. C. Wu, J. L. Gottfried, R. A. Pesce-Rodriguez, On the structure and impurities of a nominally homologous set of detonation nanodiamonds, *Diam. Relat. Mater.* 76 (2017) pp 157-170.

- [61] A.R. Kirmani, W. Peng, R. Mahfouz, A. Amassian, Y. Losovyj, H. Idriss, K. Katsiev, On the relation between chemical composition and optical properties of detonation nanodiamonds, *Carbon* 94 (2015) pp 79-84.
- [62] Y. Liu, Z. Gu, John L. Margrave, V. N. Khabashesku, Functionalization of Nanoscale Diamond Powder: Fluoro-, Alkyl-, Amino-, and Amino Acid-Nanodiamond Derivatives, *Chem. Mater.* 16 (2004) pp 3924-3930.
- [63] A. N. Utyuzh, Y. A. Timofeev, A. V. Rakhmanina, Effect of Boron Impurity on the Raman Spectrum of Synthetic Diamond, *Inorganic Materials* 40 (2004) pp 926-931.
- [64] S. Heyer, W. Janssen, S. Turner, Y.G. Lu, W.S. Yeap, J. Verbeeck, K. Haenen, A. Krueger, Toward deep blue nano hope diamonds: heavily boron-doped diamond nanoparticles. *ACS Nano* 8 (2014) pp 5757-5764.
- [65] J. C. Arnault, H. A. Girard, Hydrogenated nanodiamonds: Synthesis and surface properties, *Current Opinion in Solid State and Materials Science*, 21 (2017) pp 10–16.
- [66] T. Kondo, I. Neitzel, V. N. Mochalin, J. Urai, M. Yuasa, Y. Gogotsi, *J. Appl. Phys.* 113 (2013) 214307 1-5.
- [67] E. Maillard-Schaller, O. M. Kuettel, L. Diederich, L. Schlapbach, V. V. Zhirnov, P. I. Belobrov, Surface properties of nanodiamond films deposited by electrophoresis on Si(100), *Diam. Relat. Mater.* 8 (1999) pp 805-808.
- [68] A. Bolker, C. Saguy, R. Kalish, Transfer doping of single isolated nanodiamonds, studied by scanning probe microscopy techniques, *Nanotechnology* 25 (2014) 385702.
- [69] E. Vanhove, J. de Sanoit, J. C. Arnault, S. Saada, C. Mer, P. Mailley, P. Bergonzo, M. Nesladek, Stability of H-terminated BDD electrodes: an insight into the influence of the surface preparation, *phys. Stat. sol. (a)* 204 (2007) pp 2931-2939.
- [70] A. Krüger, Y. Liang, G. Jarre, J. Stegk, Surface functionalisation of detonation diamond suitable for biological applications. *J. Mater. Chem.* 16 (2006) pp 2322–2328.
- [71] S. Osswald, G. Yushin, V. Mochalin, S.O. Kucheyev, Y. Gogotsi, Control of sp<sup>2</sup>/sp<sup>3</sup> carbon ratio and surface chemistry of nanodiamond powders by selective oxidation in air, *J. Am. Chem. Soc.* 128 (2006) pp 11635–11642.
- [72] L. S. Sundar, M. J. Hortiguera, M. K. Singh, A. C.M. Sousa, Thermal conductivity and viscosity of water based nanodiamond (ND) nanofluids: An experimental study, *International Communications in Heat and Mass Transfer* 76 (2016) 245–255
- [73] M. Comet, V. Pichot, B. Siegert, F. Britz, D. Spitzer, Detonation nanodiamonds for doping Kevlar, *J. Nanosci. Nanotechnol.* 10 (2010) pp 4286-4292.
- [74] O. Shenderova, A.M. Panich, S. Moseenkov, S.C. Hens, V. Kuznetsov, H.M. Vieth, Hydroxylated detonation nanodiamond: FTIR, XPS, and NMR studies. *J. Phys. Chem. C* 115 (2011) pp 19005–19011.
- [75] R. Martín, M. Álvaro, J.R. Herance, H. García, Fenton-treated functionalized diamond nanoparticles as gene delivery system. *ACS Nano* 4 (2010) pp 65–74.

- [76] G. Cunningham, A.M. Panich, A.I. Shames, I. Petrov, O. Shenderova, Ozone-modified detonation nanodiamonds, *Diam. Relat. Mater.* 17 (2008) pp 650-654.
- [77] O. Shenderova, A. Koscheev, N. Zaripov, I. Petrov, Y. Skryabin, P. Detkov, T. Turner, G. Van Tendeloo, Surface chemistry and properties of ozone-purified detonation nanodiamonds. *J. Phys. Chem. C* 115 (2011) pp 9827–9837.
- [78] T. Petit, J. C. Arnault, H. A. Girard, M. Sennour, P. Bergonzo, Early stages of surface graphitization on nanodiamond probed by X-ray photoelectron spectroscopy, *Phys. Rev. B* 84 (2011) 233407 1-5.
- [79] Y.V. Butenko, S. Krishnamurthy, A.K. Chakraborty, V.L. Kuznetsov, V.R. Dhanak, M.R.C. Hunt, L. Scaroniller, L. Šiller, Photoemission study of onionlike carbons produced by annealing nanodiamonds. *Phys. Rev. B* 71(7), 75420 (2005).
- [80] A.T. Dideikin, A.E. Aleksenskii, M.V. Baidakova, P.N. Brunkov, M. Brzhezinskaya, V. Yu. Davydov, V.S. Levitskii, S.V. Kidalov, Yu. A. Kukushkina, D.A. Kirilenko, V.V. Shnitov, A.V. Shvidchenko, B.V. Senkovskiy, M.S. Shestakov, A. Ya. Vul', Rehybridization of carbon on facets of detonation diamond nanocrystals and forming hydrosols of individual particles, *Carbon* 122 (2017) pp 737-745.
- [81] J. Havlik, H. Raabova, M. Gulka, V. Petrakova, M. Krecmarova, V. Masek, P. Lousa, J. Stursa, H. G. Boyen, M. Nesladek, P. Cigler, Benchtop Fluorination of Fluorescent Nanodiamonds on a Preparative Scale: Toward Unusually Hydrophilic Bright Particles, *Adv. Funct. Mater.* 26 (2016) pp 4134-4142.
- [82] S. Sotoma, K. Akagi, S. Hosokawa, R. Igarashi, H. Tochio, Y. Harada, M. Shirakawa, Comprehensive and quantitative analysis for controlling the physical/chemical states and particle properties of nanodiamonds for biological applications, *RSC Adv.* 5 (2015) pp 13818-13827.
- [83] S. C. Hens, G. Cunningham, T. Tyler, S. Moseenkov, V. Kuznetsov, O. Shenderova, Nanodiamond bioconjugate probes and their collection by electrophoresis, *Diam. Relat. Mater.* 17 (2008) pp 1858-1866.
- [84] H. A. Girard, T. Petit, S. Perruchas, T. Gacoin, C. Gesset, J. C. Arnault, P. Bergonzo, Surface properties of hydrogenated nanodiamonds: a chemical investigation, *Phys. Chem. Chem. Phys.* 13 (2011) p 11517-11523.
- [85] V. R. Dhanak, Yu. V. Butenko, A. C. Brieva, P. R. Coxon, L. Alves, L. Šiller, Chemical Functionalization of Nanodiamond by Amino Groups: An X-Ray Photoelectron Spectroscopy Study, *J. Nanoscience and Nanotechnology* 12 (2012) pp 3084-3090.
- [86] J. R. Bertrand, C. Pioche-Durieu, J. Ayala, T. Petit, H. A. Girard, C. P. Malvy, E. Le Cam, F. Treussart, J. C. Arnault, Plasma hydrogenated cationic detonation nanodiamonds efficiently deliver to human cells in culture functional siRNA targeting the Ewing sarcoma junction oncogene, *Biomaterials* 45 (2015) pp 93-98.
- [87] C. Gaillard, H. A. Girard, C. Falck, V. Paget, V. Simic, N. Ugolin, P. Bergonzo, S. Chevillard, J. C. Arnault, Peptide nucleic acid–nanodiamonds: covalent and stable conjugates for DNA targeting, *RSC Adv.* 4 (2014) pp 3566-3572.

- [88] S. A. Dahoumane, M. N. Nguyen, A. Thorel, J. P. Boudou, M. M. Chehimi, C. Mangeney, Protein-Functionalized Hairy Diamond Nanoparticles, *Langmuir* 25 (2009) pp 9633-9638.
- [89] C. Mangeney, Z. Qin, S. A. Dahoumane, A. Adenier, F. Herbst, J. P. Boudou, J. Pinson, M. M. Chehimi, Electroless ultrasonic functionalization of diamond nanoparticles using aryl diazonium salts *Diam. Relat. Mater* 17 (2008) pp 1881-1887.
- [90] X. Zhang, Fu, L. Feng, Y. Ji, L. Tao, Q. Huang, S. Li, Y. Wei, PEGylation and polyPEGylation of nanodiamond, *Polymer* 53 (2012) pp 3178-3184.
- [91] M. Yeganeh, P. Coxon, A. Brieva, V. Dhanak, L. Šiller, Y. Butenko, Atomic hydrogen treatment of nanodiamond powder studied with photoemission spectroscopy. *Phys. Rev. B* 75 (2007) 155404 pp 1–8.
- [92] P.I. Belobrov, L.A. Bursill, K.I. Maslakov, A.P. Dementjev, Electron spectroscopy of nanodiamond surface states, *Appl. Surf. Science* 215 (2003) pp 169-177.
- [93] J. C. Arnault, T. Petit, H. A. Girard, A. Chavanne, C. Gesset, M. Sennour, M. Chaigneau, Surface chemical modifications and surface reactivity of nanodiamonds hydrogenated by CVD plasma, *Phys. Chem. Chem. Phys.* 13 (2011) pp 11481-11487.
- [94] J. C. Arnault, H. A. Girard, Diamond nucleation and seeding techniques: two complementary strategies for growth of ultra-thin diamond films, in *Nanodiamonds*, Royal Society Chemistry, ed. by O. A. Williams (2014), pp. 221–252. ISBN 978-1-84973-639-8
- [95] J.C. Arnault, S. Saada, O.A. Williams, K. Haenen, P. Bergonzo, M. Nesladek, R. Polini, E. Osawa, Diamond nanoseeding on silicon: stability under H<sub>2</sub> MPCVD exposures and early stages of growth. *Diam. Relat. Mater.* 17 (2008) pp 1143–1149.
- [96] J.C. Arnault, S. Saada, O.A. Williams, K. Haenen, P. Bergonzo, M. Nesladek, R. Polini, E. Osawa, Surface characterisation of silicon substrates seeded with diamond nanoparticles under UHV annealing. *Phys. Stat. Sol. (A)* 205 (2008) pp 2108–2113.
- [97] S. Zeppilli, J. C. Arnault, C. Gesset, P. Bergonzo, R. Polini, Thermal stability and surface modifications of detonation diamond nanoparticles studied with X-ray photoelectron spectroscopy, *Diam. Relat. Mater.* 19 (2010) p 846-853.
- [98] J.Y. Raty, G. Galli, C. Bostedt, T.W. van Buuren, L.J. Terminello, Quantum confinement and fullerene-like surface reconstructions in nanodiamonds. *Phys. Rev. Lett.* 90 (2003) 37401.
- [99] Y. Liang, T. Meinhardt, G. Jarre, M. Ozawa, P. Vrdoljak, A. Schöll, F. Reinert, A. Krueger, Deagglomeration and surface modification of thermally annealed nanoscale diamond, *J. Colloid Interface Sci.* 354 (2011) pp 23–30.
- [100] S. Krishnamurthy, Yu.V. Butenko, V.R. Dhanak, M.R.C. Hunt, L. Siller, In situ formation of onion-like carbon from the evaporation of ultra-dispersed nanodiamonds, *Carbon* 52 (2013) pp 145-149.
- [101] F. Maier, R. Graupner, M. Hollering, L. Hammer, J. Ristein, L. Ley, *Surf. Science* 443 (1999) pp 177-185.
- [102] F. Maier, M. Riedel, B. Mantel, J. Ristein, L. Ley, Origin of surface conductivity of diamond, *Phys. Rev. Lett.* 85 (2000) pp 3472-3475.

- [103] T. Petit, H. Yuzawa, M. Nagasaka, R. Yamanoi, E. Osawa, N. Kosugi, E. F. Aziz, Probing Interfacial Water on Nanodiamonds in Colloidal Dispersion, *J. Phys. Chem. Lett.* 6 (2015) pp 2909–2912.
- [104] T. Petit, L. Puskar, T. A. Dolenko, S. Choudhury, E. Ritter, S. Burikov, K. Laptinskiy, Q. Brzustowski, U. Schade, H. Yuzawa, M. Nagasaka, N. Kosugi, M. Kurzyp, A. Venerosy, H. A. Girard, J.-C. Arnault, E. Osawa, N. Nunn, O. Shenderova and E. F. Aziz, Unusual Water Hydrogen Bond Network around Hydrogenated Nanodiamonds, *J. Phys. Chem. C* 121 (2017) pp 5185-5194.
- [105] Y. C. Lu, E. J. Crumlin, G. M. Veith, J. R. Harding, E. Mutoro, L. BAggetto, N. J. Dudney, Z. Liu, Y. Shao-Horn, In Situ Ambient Pressure X-ray Photoelectron Spectroscopy Studies of Lithium-Oxygen Redox Reactions, *Scientific Report* 2 (2012) 715.
- [106] S. Benkoula, O. Sublemontier, M. Patanen, C. Nicolas, F. Sirotti, A. Naitabdi, F. Gaie-Levrel, E. Antonsson, D. Aureau, F. X. Ouf, S. I. Wada, A. Etcheberry, K. Ueda, C. Miron, Water adsorption on TiO<sub>2</sub> surfaces probed by soft X-ray spectroscopies: bulk materials vs. isolated nanoparticles, *Scientific Reports* 5 (2015) 15088.